

ORIGINAL RESEARCH

Open Access



Evolution and correlation of the physiochemical properties of bamboo char under successive pyrolysis process

Jiajun Wang¹, Zhenrui Li¹, Yujun Li¹, Zhihui Wang¹, Xing'e Liu¹, Zhenzhen Liu¹ and Jianfeng Ma^{1*}

Abstract

This study investigated the effects of bamboo age, bamboo parts, and pyrolysis temperatures on the physiochemical properties of bamboo char throughout a series of pyrolysis processes spanning from 150 °C to 1000 °C. The results indicated that as the pyrolysis temperature increased from 150 °C to 500 °C, the yield of bamboo char experienced a rapid decline, settling at a maximum of 69%, with no significant impact from bamboo age and parts. Subsequently, as the pyrolysis temperature continued to rise from 500 °C to 1000 °C, the yield stabilized at 25.74–32.64%. Besides, fixed carbon (FC), volatile matter (VM), and ash content were temperature-dependent, while the H/C, O/C, (N+O)/C, and aromatic index kept constant after reaching 500 °C. Notably, 800 °C was confirmed to be a crucial turning point for physiochemical properties, at which the graphitic structural changes occurred, pore collapsed, and potassium salts released. Bamboo age was proved to enhance the stability. Pearson correlation coefficient (PCC) analysis revealed that the pyrolysis temperature was positively correlated ($p < 0.01$) with ash (0.76), FC (0.97), AI (0.81), R_{50} (0.77), and $C-C/C=C/C-H$ (0.87). Conversely, negative correlations ($p < 0.01$) were observed with VM (−0.91), O/C (0.88), H/C (−0.95), (N+O)/C (−0.87), C loss (−0.79), and labile organic-C (−0.78). Additionally, bamboo age was negatively correlated ($p < 0.01$) with C loss (−0.40), volatile organic-C (−0.63), labile organic-C (−0.45), and recalcitrant organic-C (−0.40), but positively associated with R_{50} (0.54), refractory organic-C (0.42), and inorganic-C (0.52). Bamboo parts did not exhibit significant correlations with char properties.

Highlights

- 500 °C and 800 °C served as key turning points for the properties of biochar.
- Bamboo age had a positive effect on thermal stability and chemical stability.
- There was no significant difference in properties between different parts (internodes and nodes) of bamboo.

Keywords Bamboo char, Temperature, Physicochemical properties, Evolution, Correlation

Handling editor: Jun Meng

*Correspondence:

Jianfeng Ma

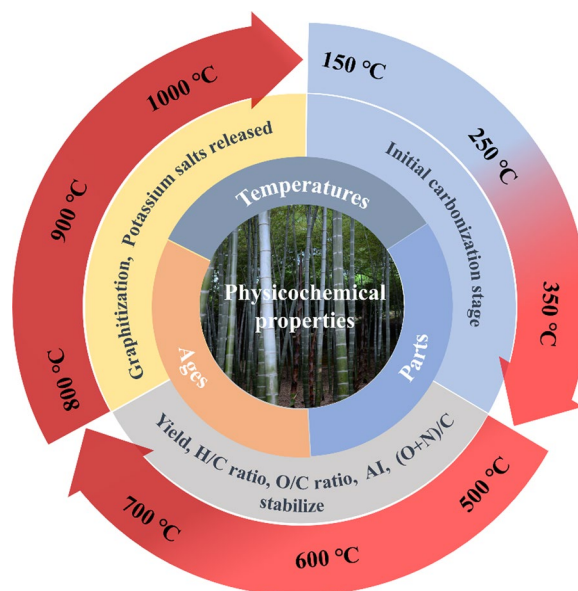
Majf@icbr.ac.cn

Full list of author information is available at the end of the article



© The Author(s) 2024. **Open Access** This article is licensed under a Creative Commons Attribution 4.0 International License, which permits use, sharing, adaptation, distribution and reproduction in any medium or format, as long as you give appropriate credit to the original author(s) and the source, provide a link to the Creative Commons licence, and indicate if changes were made. The images or other third party material in this article are included in the article's Creative Commons licence, unless indicated otherwise in a credit line to the material. If material is not included in the article's Creative Commons licence and your intended use is not permitted by statutory regulation or exceeds the permitted use, you will need to obtain permission directly from the copyright holder. To view a copy of this licence, visit <http://creativecommons.org/licenses/by/4.0/>.

Graphical Abstract



1 Introduction

Biochar, a carbonaceous material derived from the pyrolysis of biomass, has gained significant interest as a promising material with unique physicochemical properties (Li et al. 2017; Shaheen et al. 2018; Weldon et al. 2019). The physicochemical properties of biochar can be influenced by several processing factors (Dong et al. 2023; Lian et al. 2023; Wang et al. 2023b), with the pyrolysis temperature considered a determining parameter (Pradhan et al. 2020).

Temperature plays a crucial role in shaping the properties and potential applications of biochar (de Almeida et al. 2022; Fan et al. 2023; Zhou et al. 2021). Biochar shows varying degrees of carbonization due to variations in pyrolysis temperature and possesses highly ordered aromatic structures when the temperature exceeds 400 °C (Kim et al. 2012). Furthermore, elevating the temperature facilitates the transformation of biochar into a more graphitic structure. On increasing the charring temperature from 100 °C to 700 °C, biochar experienced four distinct char phases and physical states in turn, including transitional char, amorphous char, composite char, and turbostratic char (Keiluweit et al. 2010). Beyond 700 °C, the structure of biochar further evolves, leading to the formation of graphitized biochar (Zhang et al. 2021a). This enhancement of graphitization level can not only promote their electron transfer capacity and electrical

conductivity (Gabhi et al. 2020; Tonnoir et al. 2023) but also influence its adsorption and catalytic activities (Wan et al. 2021; Wang et al. 2023a). Additionally, increased graphitization can stimulate microbial growth, thereby facilitating anaerobic digestion capacity for waste (Zhang et al. 2022a; Zhou et al. 2021). In a practical example, Yang et al. (2018) utilized bamboo processing residues to produce highly graphitized biochar with an impressive sulfur removal rate of 96%. A higher degree of graphitization results in a more ordered structure of biochar, expanding the conjugated π electron system and further increasing its adsorption capacity (Hou et al. 2021).

Moreover, increasing the pyrolysis temperature induces dehydration, decarboxylation, and decarbonylation reactions in biomass, leading to a reduction in H/C and O/C ratios of biochar. These two ratios play a crucial role in determining the chemical composition and reactivity of biochar (Weber and Quicker 2018). The H/C ratio reflects the hydrogen content relative to carbon, offering insights into the carbonization and aromaticity. Meanwhile, the O/C ratio indicates the oxygen content and influences the hydrophilicity and thermal stability of biochar. By manipulating these ratios through varying pyrolysis conditions or feedstock types, properties of biochar can be tailored to specific applications, such as soil improvement, water treatment, and carbon sequestration. Remarkably, biochar has demonstrated its effectiveness in reducing

N_2O emissions from soils, with the H/C ratio identified as a crucial determinant of its N_2O mitigation potential. Biochars with $\text{H/C} < 0.3$ have proven to be highly effective in this regard (Cayuela et al. 2015). Additionally, biochar characterized by high aromatic carbon content and low O/C and H/C ratios is more suitable for applications like soil carbon sequestration (Wang et al. 2015). Meanwhile, the H/C and O/C ratios serve as essential parameters for predicting the adsorption performance of biochar. Research has reported that raising the pyrolytic temperature could increase the aromaticity and hydrophobicity of biochar while expanding its surface area, which facilitated its adsorption for various organic compounds (Kearns et al. 2014; Shimabuku et al. 2016; Sun et al. 2016). Zhao et al. (2019) demonstrated that the higher hydrophobicity of biochar enhanced the atrazine adsorption. Wei et al. (2020) established the H/C ratio as a predictive parameter for the adsorption mechanism of the herbicide metolachlor on biochar. Besides, extensive work has clearly identified the crucial role of the aromatic moiety in biochar for its stability (Han et al. 2020) and efficiency in adsorbing polar and nonpolar hydrophobic organic contaminants (HOCs) (Chu et al. 2019; Tan et al. 2015).

Furthermore, temperature exhibits a pronounced impact on the surface roughness, micromorphology, and porous structure of biochar (Gupta et al. 2019; Wang et al. 2019). Meanwhile, it influences some parameters such as electrical conductivity (EC) and pH (Chen et al. 2019; Meier et al. 2015). Vigišová et al. (2018) produced bamboo biochar at 460 °C, with a specific surface area of only 28 $\text{m}^2 \text{g}^{-1}$, primarily characterized by macropores and micropores. In contrast, Hien et al. (2020) investigated different pyrolysis temperatures and retention times for bamboo biochar and found that higher temperatures and extended retention times increased the specific surface area and water-holding capacity. Zhang et al. (2021b) investigated the influence of pyrolysis temperature on the physicochemical properties of bamboo material and revealed that bamboo biochar prepared at 850 °C exhibited a surface area of 382.8 $\text{m}^2 \text{g}^{-1}$. Collectively, these research findings suggest that pyrolysis temperatures exceeding 450 °C are necessary to produce highly porous biochar with an enlarged surface area. In a study by Suthar et al. (2018), the pyrolysis of bamboo at different temperatures (300, 450, and 600 °C) unveiled that bamboo biochar produced at 600 °C possessed the highest specific surface area, reaching 247.2 $\text{m}^2 \text{g}^{-1}$.

Bamboo offers several advantages over wood, such as rapid growth, a short harvest cycle typically ranging from 3 to 5 years (Iroegbu and Ray 2021), and lower

ash content compared to rice husk biomass, making it an ideal candidate for biochar production. Moreover, bamboo forests possess a greater carbon sequestration capacity than ordinary trees, being 1.46 times that of fir forests (*Cunninghamia lanceolata*) and 1.33 times that of tropical rainforests (Li et al. 1998; Ruan et al. 1997; Xu et al. 2020; Yen and Lee 2011). The conversion of bamboo into biochar can further mitigate carbon emissions and bolster its carbon sequestration potential (Li et al. 2018a; Nath et al. 2015). As bamboo grows, variations in the accumulation of components may occur in different parts of the bamboo. These may include differences in the distribution of various forms of organic and inorganic carbon, as well as the presence of other essential elements. Such variations in components are likely to be reflected in the biochar production process, significantly affecting the physicochemical properties of the resulting biochar. Studies have shown that the pyrolysis of bamboo is influenced by the age of the bamboo (Cheng et al. 2015; Hossain et al. 2022), with an extended growth period resulting in reduced cellulose content and increased lignin and ash content. Additionally, thermogravimetric analyses have revealed distinct thermal degradation patterns for different parts of the bamboo stem and leaves (Liang et al. 2018). However, it is important to recognize that most existing research has concentrated on pyrolyzing bamboo under a single set of conditions to produce biochar and has focused on evaluating its physicochemical characteristics or carbon stability (Chen et al. 2016; Mu et al. 2023). There is an urgent need for comprehensive studies to establish correlations among various factors determining the properties of the produced biochar. This will favor the targeted production of biochars for practical applications.

This work prepared a series of biochars using *moso* bamboo (*Phyllostachys pubescens*) of varying ages (1, 2, 3, and 4 years) at nine pyrolysis temperatures (i.e., 150, 250, 350, 500, 600, 700, 800, 900, and 1000 °C). Meanwhile, it investigated the impacts of temperature, bamboo age, and bamboo parts (internodes and nodes) on the physicochemical properties of biochar. Additionally, it conducted an in-depth analysis of the correlations between these distinct physicochemical properties and the temperature changes, bamboo age, and bamboo parts (internodes and nodes). The primary objectives of this study were (1) to scrutinize how temperature, bamboo age, and bamboo parts (internodes and nodes) affect the physicochemical attributes of biochar; and (2) to elucidate the patterns of variation in H/C, O/C, and degree of graphitization of the biochar. The findings of this study are expected to enhance our understanding of how bamboo age and bamboo parts shape the properties of biochar, facilitating its effective utilization in diverse fields.

2 Materials and methods

2.1 Materials

Moso bamboo (*Phyllostachys pubescens*) specimens were collected from the Taiping Experimental Center of the International Center for Bamboo and Rattan in Anhui Province, China. The internodal samples were taken from the bamboo at the 1.5 m position, while the nodal samples were obtained from the nearest nodes both above and below the 1.5 m mark. Internodes and nodes were carefully harvested and cut into pieces of approximately 10 mm (width) × 10 mm (thickness) × 20 mm (length). Then, these pieces were subjected to drying at 103 ± 2 °C for 12 h until they reached a constant weight. A two-step process involving dilute acid and enzyme lignin (DEL) treatments was employed to prepare the original lignin of both bamboo fiber cells and parenchyma cells. Subsequently, holocellulose material was extracted from these bamboo cell types, followed by the separation of hemicelluloses and cellulose components from the holocellulose material.

2.2 Pyrolysis process

The specimen pieces underwent further processing with pyrolysis in a resistance furnace at target temperatures of 150, 250, 350, 500, 600, 700, 800, 900, and 1000 °C in a controlled N₂ atmosphere for 2 h. Afterwards, the furnace was allowed to naturally cool to room temperature. The N₂ flow remained open throughout the entire pyrolysis and cooling process to prevent oxidation of the samples at high temperatures. The slow pyrolysis heating rate was set to 5 °C min⁻¹, starting at an initial temperature of 30 °C. The resulting solid products, i.e., biochar, were stored in a desiccator and sealed in plastic bags. To facilitate distinction, the biochar samples were labeled with an abbreviation followed by the pyrolysis temperature. For example, “1Y-BC150-I” represents the biochar obtained from the internode section of 1-year-old bamboo pyrolyzed at 150 °C, while “BC150-N” refers to the biochar sample derived from the bamboo nodes at a pyrolysis temperature of 150 °C.

2.3 Biochar characterization

The specific surface area of the biochar was determined by performing N₂ adsorption/desorption isotherms at 77 K using a surface area analyzer (Brunauer–Emmett–Teller (BET), BELSORP-mini, Japan). The NLDFT was used to calculate the pore size distribution. The proximate analysis, which included ash, volatile matter (VM), and fixed carbon (FC) of the bamboo and biochars, adhered to the national standard GB/T 28731–2012. Elemental analysis (EA) (SDCHN435, Sundry, China) was performed to estimate the CHON content in the biochar samples. In addition, the atomic ratios of H/C, O/C and (N+O)/C were calculated to characterize the properties of the biochar. The aromaticity index (AI) of the biochar

was also calculated using the following equation (Xu et al. 2021; Zhrebker et al. 2022):

$$AI = \frac{1 + [C] - [O] - 0.5[H]}{[C] - [O] - [N]} \quad (1)$$

The composition and chemical state of elements on the surfaces of the samples were analyzed using X-ray photoelectron spectroscopy (XPS) with Al K α radiation (Thermo Fisher escalab, 250xi, USA). High-resolution XPS spectra in the C 1s region were deconvoluted to quantify different carbon forms, with the binding energy of the spectra calibrated at 284.8 eV. Besides, the morphologies of fabricated biochar were studied using a scanning electron microscopy (SEM)/energy dispersive spectrometer (EDS) (GeminiSEM360, Zeiss, Germany). X-Ray diffractometer (XRD-6100, Shimadzu, Japan) was employed to examine the crystalline structure of biochar. Additionally, the graphitization of the biochars was probed by a transmission electron microscope (TEM, Thermo Fisher Talos F200X, USA).

2.4 Evolved gas analysis

Evolved gas analysis involves measuring the gases released during the heating of a sample by a thermal analyzer (Zeng et al. 2015). These gases can originate from various processes, such as evaporation, boiling, separation, or the combustion/pyrolysis of material. It is often performed using hyphenated techniques, where two or more instruments are combined to significantly improve analytical capabilities. This method not only deepens the level of analysis but also optimizes time efficiency by extracting more information in a single run. For this study, a coupled TG and FTIR apparatus was used for the pyrolysis experiments, with the parameters aligned with those of the tube furnace. The focus was on analyzing the gas composition during the pyrolysis of biomass samples, specifically cellulose, hemicelluloses, and lignin. Thermogravimetric analysis (TGA4000, PerkinElmer, USA) was conducted in an inert (N₂) atmosphere with a heating rate of 5 °C min⁻¹, using approximately 10 mg of dried bamboo powder, cellulose, hemicelluloses, and lignin placed in the sample holder. The pyrolysis temperature spanned from room temperature to 800 °C, and TG-DTG curves were recorded within this range. Online FTIR analysis was performed on the gases evolved during the pyrolysis process. The transfer line (TL800, PerkinElmer, USA) between the TGA and FTIR was maintained at a temperature of 280 °C to prevent the condensation of volatile substances.

The evolved gases were analyzed online by Fourier transform infrared spectroscopy (Spotlight400, PerkinElmer, USA), which was conducted in the range of

4000–400 cm^{-1} with an interval of 1 cm^{-1} . Pure nitrogen was used as the carrier gas at a flow rate of 20 mL min^{-1} . The FTIR absorption was recorded throughout the experimental process, and finally, 3D FTIR absorption spectra were established correlating pyrolysis temperature and wavenumber. Specific compound absorption peaks such as H_2O , CH_4 , CO_2 , CO , and compounds containing $\text{C}=\text{O}$ bonds were also extracted from the 3D FTIR spectra to illustrate their variation throughout the pyrolysis process.

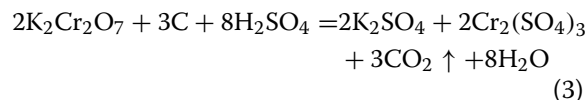
2.5 Stability of biochar for thermal-oxidation resistance and chemical-oxidation resistance

The thermal-oxidation resistance of the biochar was evaluated following established procedures as previously reported (Leng et al. 2019; Yang et al. 2016). Weight loss attributed to the thermal oxidation was monitored in an air environment using thermogravimetry/derivative thermogravimetry (TG/DTG). The thermal analysis was initiated at 30 °C, with a ramping rate of 10 °C min^{-1} to 800 °C. An indicator (R_{50}) was employed to gauge the oxidation recalcitrance of biochar during TG analysis (Eq. 2) (Harvey et al. 2012) with graphite as the reference. It's noteworthy that the fixed value for T_{50} of graphite is 886 °C (Harvey et al. 2012).

$$R_{50,\text{biocahr}} = \frac{T_{50,\text{biochar}}}{T_{50,\text{graphite}}} \quad (2)$$

The chemical-oxidation resistance of the biochar was evaluated employing the $\text{K}_2\text{Cr}_2\text{O}_7$ oxidation method at 55 °C for 60 h in triplicates (Leng et al. 2019; Nan et al. 2020). Approximately 0.1 g of biochar was added into a glass test tube containing 40 mL of 0.1 M $\text{K}_2\text{Cr}_2\text{O}_7/2$ M H_2SO_4 solution. To determine the extent of carbon loss, the transition of Cr (VI) concentration was monitored using Eq. (3). Furthermore, the proportion of carbon loss

was calculated based on the carbon content in the biochar detected by EA.



2.6 Pearson correlation coefficient analysis

IBM SPSS Statistics 26 software was utilized to conduct Pearson correlation coefficient analyses, examining the relationships between various pyrolysis temperatures, bamboo ages, and bamboo parts (internodes and nodes) concerning the fundamental properties of bamboo biochar. The study focused on assessing resistance to thermal oxidation and chemical stability through R_{50} values and C loss. Additionally, other parameters, such as the proximate analysis of biochars, H/C, O/C, (N+O)/C, AI, C–C/C=C/C–H ratios, and ratios of different carbon types based on TG analysis, were included in the analysis.

3 Result and discussion

3.1 Yield and proximate analyses of biochars

The effects of pyrolysis temperature on the biochar yield and TG analysis are presented in Fig. 1. The pyrolysis temperature exerted a substantial influence on the biochar yield. As the temperature increased from 150 °C to 500 °C, there was a pronounced decrease in yield across all samples, dropping from 99.19–100% to 31.28–32.64% (Fig. 1a). However, there was no significant variation within the temperature range of 500–1000 °C, and the yield remained 32.64–25.74%. Zhang et al. (2017) studied the pyrolysis of bamboo at a heating rate of 10 °C min^{-1} from 200 °C to 800 °C, and the yield of biochar obtained was similar to that of this study. Sahoo et al. (2021) also obtained similar results in their research. This indicated that the influence of pyrolysis temperature on yield is the

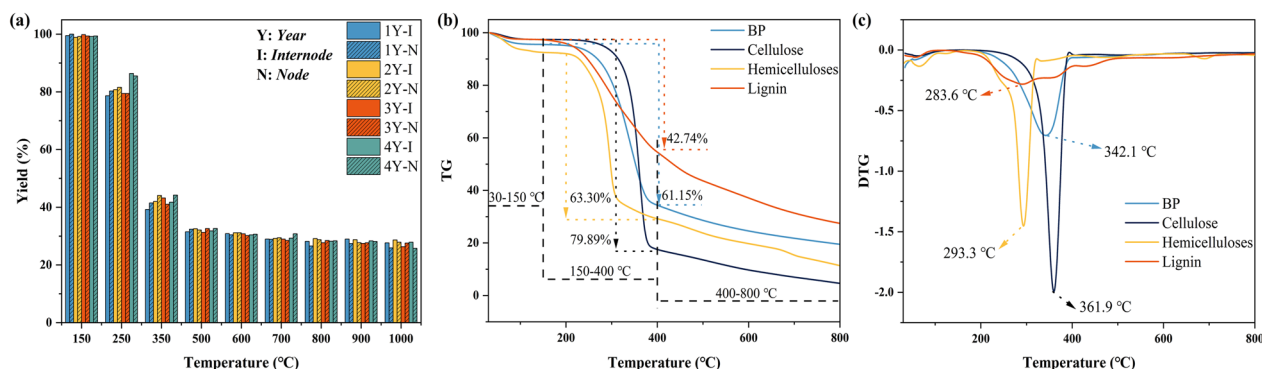


Fig. 1 Yield of internodes and nodes of bamboo varies across different ages and temperatures (a). TG analysis of bamboo powder (BP), cellulose, hemicelluloses and lignin (b). DTG curves of bamboo powder (BP), cellulose, hemicelluloses and lignin (c). 1Y-I and 1Y-N represent internodes and nodes of 1-year-old, respectively, in (a)

most significant factor. Notably, the yield showed no discernible difference with respect to bamboo age or bamboo parts (Fig. 1a). The TG/DTG curves depicting the cellulose, hemicelluloses, lignin of bamboo, and bamboo powder (BP) are displayed in Fig. 1b and c. The pyrolysis processes of all three components and BP exhibited three stages (Fig. 1c). As the samples were pre-dried, the weight loss rate during the first stage (Stage I, 30–150 °C) was very low (2.58–7.49%). During the second stage (Stage II, 150–400 °C), characterized by rapid decomposition, the samples underwent thermal cracking reactions, resulting in significant weight loss (42.74–79.89%). The third stage (Stage III 400–800 °C) marked a slow thermal cracking of the samples, ultimately yielding the biochar with yields of 4.64%, 11.36%, and 27.48% for cellulose, hemicelluloses, and lignin, respectively.

Nevertheless, the thermal stability and thermogravimetric behavior of the three biomass components are greatly different. Specifically, hemicelluloses demonstrate the lowest initial thermal decomposition temperature (192.6–324.9 °C) with a sharp peak at 293.3 °C. In contrast, cellulose takes place pyrolysis at relatively high temperatures, with rapid thermal cracking reactions occurring at 236.8–392.2 °C, accompanied by a sharp peak at 361.9 °C, resulting in a weight loss of 79.9%. In contrast to hemicelluloses and cellulose, the rapid decomposition stage of lignin unfolds over a wide temperature range (163.7–502.8 °C), exhibiting a relatively lower weight loss rate of 42.9%. Lignin, with its intricate and highly branched polymer structure, possesses a complex three-dimensional arrangement that consists of building blocks with benzene rings and the most stable chemical structure among these three biomass components (Chen et al. 2022). Therefore, the biochar yield experiences a rapid decline before reaching 500 °C and tends to stabilize thereafter.

Figure 2a–c summarize the volatile matter (VM), fixed carbon (FC), and ash content of both bamboo and bamboo biochar, as determined through proximate analysis. Figure 2d–g present the TG-FTIR analysis of BP, cellulose, hemicelluloses, and lignin. The figures revealed that bamboo aged 1–4 years old predominantly consisted of VM, FC, and a small amount of ash. Specifically, VM content in both internodes and nodes ranged from 76.27% to 82.79% and 77.61% to 81.78%, respectively. The FC content varied between 15.6% and 20.57% in the internodes and 16.75% and 19.73% in the nodes. Additionally, the ash content fell within the range of 0.69% to 1.68% in the internodes and 0.62% to 1.56% in the nodes. Compared to pristine bamboo, the VM content in the biochar exhibited a significant decrease with increasing temperature from 150 °C to 500 °C, while the FC content demonstrated an opposite trend. Specifically, the VM

content dropped from 76.2–82.79% to 13.83–15.14% in the internodes and from 77.61–81.78% to 12.80–14.81% in the nodes. When the temperature was controlled at 500–1000 °C, the VM content experienced a more gradual decline, with the internodes registering a decrease from 13.83–15.14% to 2.42–3.81%, and the nodes experiencing a reduction from 12.80–14.81% to 1.77–4.47%. Simultaneously, at the same temperature conditions, the FC content in the internodes increased from 15.6–20.57% to 78.69–82.14% and rose from 16.75–19.73% to 80.17–82.79% in the nodes. Furthermore, at the range of 500–1000 °C, the FC content in the internodes enhanced from 78.69–82.14% to 88.45–93.08%, and that in the nodes rose from 80.17–82.79% to 88.72–93.30% (Fig. 2a–c). The TG-FTIR analysis (Fig. 2d–g) unveiled that the predominant volatile gases identified included H₂O, CO₂, CH₄, CO, C_xH_y, among others, with the majority of these gases being released before reaching 500 °C. The primary mass loss during bamboo pyrolysis occurs in the devolatilization stage, between 200 and 550 °C, corresponding to the main decomposition intervals of cellulose, hemicelluloses, and lignin (Wu et al. 2018; Zhang et al. 2022b). And, this observation aligns with the significant decrease in VM content observed before 500 °C. Subsequently, as the temperature continued to rise (>500 °C), only CO₂ was released.

As the temperature rose, the ash content presented an increasing trend. At the range of 150–1000 °C, the ash content of bamboo aged 1–4 years in internodes increased from 0.69–1.68% to 3.54–5.92%, and that in nodes rose from 0.62–1.56% to 3.64–5.51%. This observation suggests that elevated temperature can promote the formation and accumulation of mineral elements in the biomass, changing the ash content (Ávila et al. 2018; Nanda et al. 2015; Selvarajoo et al. 2022). However, it's noteworthy that under the same temperature and bamboo age, no obvious differences were observed in the FC content, VM content, and ash content in biochar after pyrolysis.

3.2 Ultimate analysis

The elemental analysis of both bamboo and biochars was conducted to determine atomic ratios, enabling the calculation of polarity and aromaticity. As depicted in Fig. 3a, c, e, and g, the O/C ratio for internodes of bamboo aged 1 year was 0.72, while the H/C ratio was 1.49. For nodes, the O/C and H/C ratios were 0.72 and 1.63, respectively. With increasing bamboo age, there was a corresponding rise in both the O/C and H/C ratios. For bamboo internodes aged 2, 3, and 4 years, the O/C and H/C ratios were higher by 0.03–0.04 and 0.04–0.25, respectively, compared to those aged 1 year. As for nodes, the O/C and H/C ratios for bamboo aged 2, 3, and 4 years

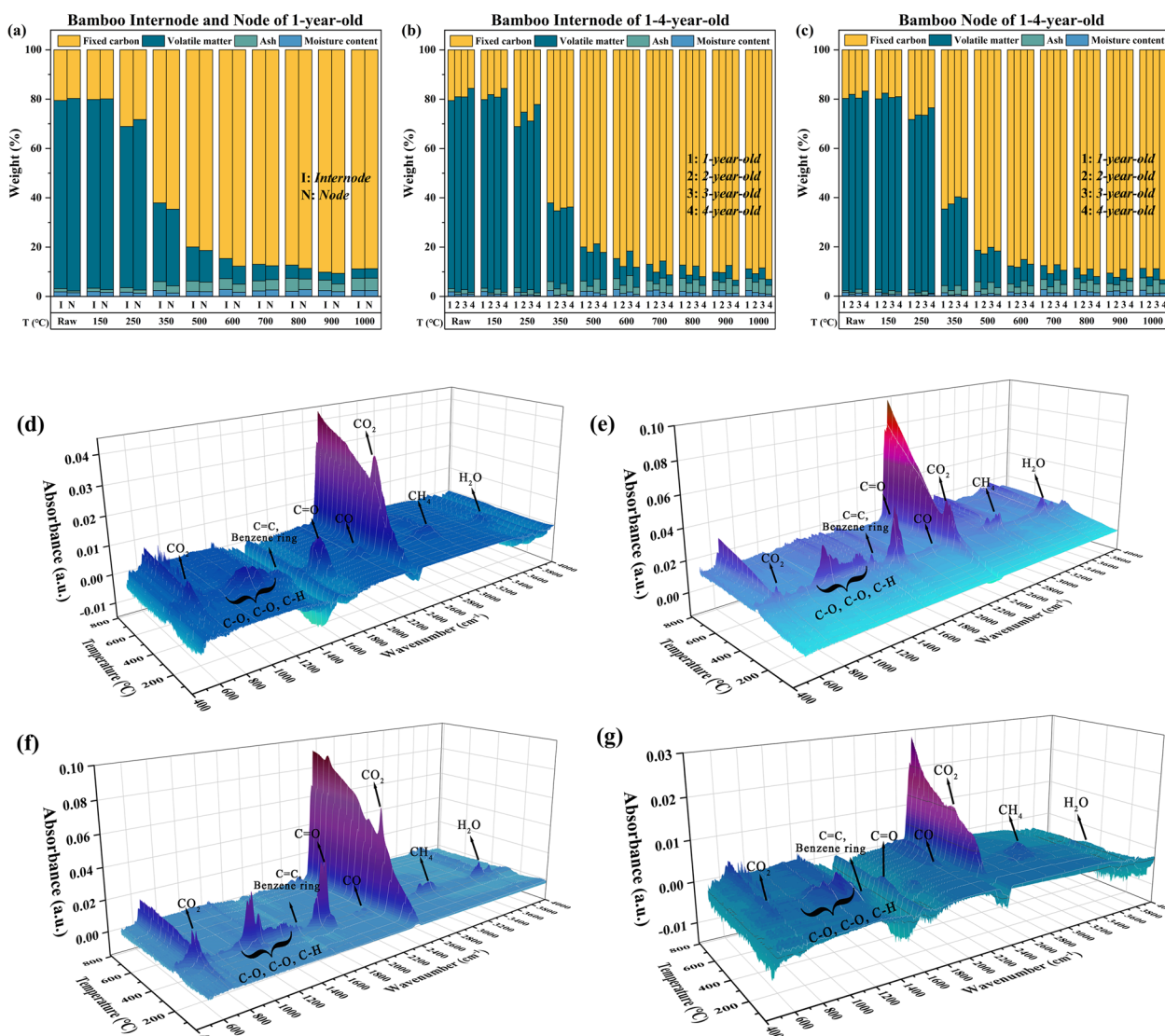


Fig. 2 Proximate analysis (volatile matter (VM), fixed carbon (FC), ash and moisture content) of internodes and nodes of 1-year-old (a); internodes of 1, 2, 3, and 4-year-old (b); nodes of 1, 2, 3, and 4-year-old (c). TG-FTIR analysis of bamboo powder (BP) (d), cellulose (e), hemicelluloses (f) and lignin (g)

were higher by 0.01–0.04 and 0.01–0.06 compared to 1-year-old bamboo, respectively.

The H/C and O/C ratios exhibited a rapid decrease when the temperature was lower than 500 °C, followed by a more gradual decline at 500–1000 °C. At 500 °C, the O/C and H/C ratios of biochars experienced a sharp decline, reaching 0.10–0.14 and 0.40–0.51, respectively. As the temperature was further increased to 1000 °C, decrease in O/C and H/C ratios slowed down, with the ranges of 0.06–0.08 and 0.02–0.05, respectively. This phenomenon was primarily attributed to dehydration, decarboxylation, and decarbonylation reactions in the biomass (Chen et al. 2022; Rodier et al. 2019). The H/C ratios

below 0.3 indicated the presence of a condensed aromatic ring, signifying an enhancement in aromaticity (de Almeida et al. 2022). Biochars with O/C ratios ranging from 0.2 to 0.6 experienced a medium carbon sequestration potential, while those with O/C ratios exceeding 0.6 were associated with a low carbon sequestration potential (Ullah et al. 2019). Notably, for all samples, the H/C and O/C ratios of the biochar were lower than those of the raw bamboo, with no significant differences between internodes and nodes.

AI was calculated using Eq. (1) to assess the evolution of aromaticity during the pyrolysis. As illustrated in Fig. 3b, d, f, and h, higher pyrolysis temperatures

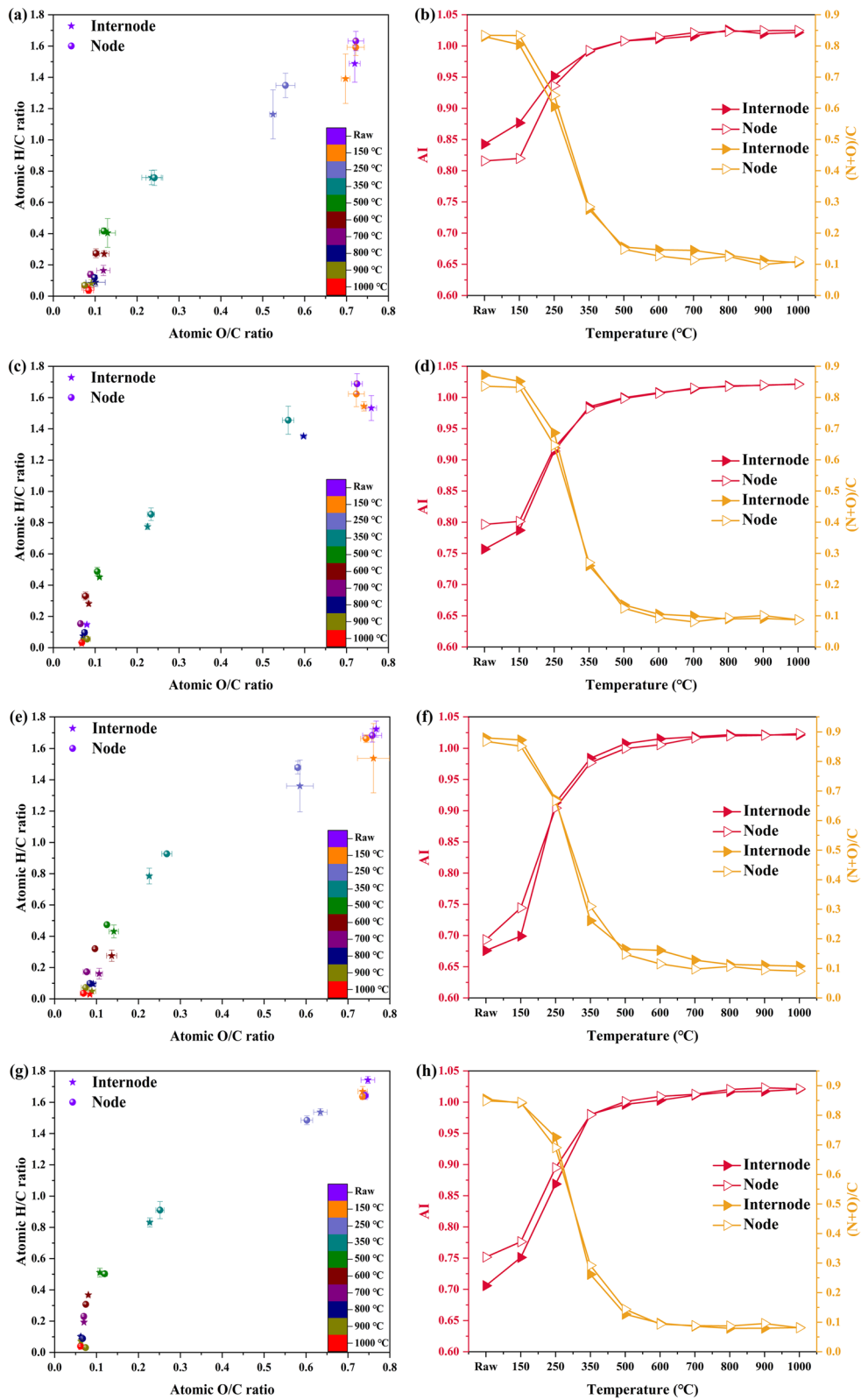


Fig. 3 The Van Krevelen diagram, AI and (N + O)/C of bamboo biochar produced at different pyrolysis temperatures and different ages: 1-year-old (a, b); 2-year-old (c, d); 3-year-old (e, f); 4-year-old (g, h)

(> 500 °C) resulted in elevated AI values (ranging of 1.00–1.02), indicating that the aromaticity was enhanced during pyrolysis. The (O+N)/C ratio defines the presence of polar functional groups (Zhang et al. 2020c). As the temperature rose to 500 °C, the polarity of biochar for bamboo aged 1–4 years sharply decreased from 0.83–0.87 to 0.12–0.17. Further increasing the temperature to 1000 °C slowed down the decrease in polarity, with the range reducing from 0.12–0.17 to 0.08–0.11. These results suggest a decrease in the content of polar functional groups but an enhancement in the hydrophobicity of the bamboo biochar.

On the other hand, the XPS analysis results revealed a gradual increase in the relative content of C–C/C=C/C–H functional groups in biochar as the temperature increased, reaching a plateau at higher temperatures (Additional file 1: Fig. S1). The content of O-containing groups in biochar fluctuated remarkably at a temperature of around 500 or 600 °C, which is consistent with the observations in the Van Krevelen diagram (Fig. 3a, c, e, and g). Dehydration and decarboxylation processes predominated when the temperature was below 500 °C, with dehydrogenation and demethylation processes becoming dominant at higher temperatures (> 500 °C). Additionally, ketones and aldehydes in carbonyl groups tend to decompose at 400–600 °C, contributing significantly to the variation in their contents. Consequently, the H and O contents in biochar decrease most rapidly with temperatures below 500 °C, with minimal changes observed after reaching 500 °C (Zhang et al. 2020a, b).

3.3 Chemical-oxidation resistance and thermal-oxidation resistance

The assessment of carbon stability and chemical oxidation resistance of bamboo and biochar involved calculating the proportion of carbon (C) loss during chemical oxidation with $K_2Cr_2O_7$ and H_2SO_4 . As depicted in Fig. 4a, at lower temperatures (< 350 °C), all the samples underwent decomposition due to oxidation. This behavior can be attributed to the inherent chemical structure of the biomass itself. At temperatures below 350 °C, the cellulose, hemicelluloses, and lignin in biomass could not be fully decomposed to form stable carbon structures, rendering them highly susceptible to oxidation by strong oxidizing agents. Biochars generated at temperatures above 350 °C displayed relatively low levels of C loss during the oxidation, with internodes and nodes experiencing C loss of 8.5–15.4% and 7.7–10.9%, respectively (Fig. 4a). Within temperature range of 350–800 °C, the internodes exhibited a higher level of C loss compared to the nodes. However, such difference became less pronounced after reaching 800 °C. At lower

temperatures, the cellulose and hemicelluloses decomposed predominantly, resulting in the formation of a higher proportion of amorphous carbon, which remained in the biochar. As the temperature increased, the lignin decomposed more obviously, contributing to the formation of high-stability aromatic carbon structures, thus counteracting the oxidation caused by an increased specific surface area and slowing down the C loss. Consequently, biochars produced at higher pyrolysis temperatures exhibited enhanced chemical oxidation stability, aligning with the results of elemental analysis, where biochar obtained at high temperatures (> 500 °C) exhibited a higher AI. High temperatures contribute to the formation of stable aromatic C with high condensation, thereby enhancing the antioxidative properties of biochar. These results align with previous research indicating that a higher pyrolysis temperature often imparts greater stability for chemical oxidation resistance (Han et al. 2018; Liu et al. 2020b; Nan et al. 2021).

Figure 4b illustrates the C loss of biochars from 1–4-year-old bamboo at 500–800 °C after chemical oxidation. At 500 °C, the C loss of biochar from bamboo aged 1 year was 15.42% for internodes and 8.97% for nodes after oxidation. Biochar derived from 2 to 4 years old bamboo exhibited lower C loss after oxidation, with the values of 13.13%, 12.94%, and 13.41% for internodes, and 6.87%, 7.21%, and 7.55% for nodes, respectively. These results indicate that the biochar from 2 to 4-year-old bamboo experienced reduced C loss compared to biochar from 1-year-old bamboo, with nodes exhibiting notably lower C loss than internodes. At 600 °C and 700 °C, the obtained biochar did not demonstrate significant regularity, likely due to the combined effects of temperature elevation. And higher temperatures enhance the aromaticity of biochar, making its structure more stable. Meanwhile, the increase in temperature results in a higher specific surface area, which, in turn, elevates the levels of C loss of biochar. At 800 °C, biochar from 1-year-old bamboo exhibited a C loss of 12.56% for internodes and that of 8.87% for nodes. In contrast, the C loss range in bamboo internodes of 2, 3, and 4-years was 11.90–12.90%, while in bamboo nodes, it fell within the range from 7.92% to 9.33%. Notably, there was no substantial difference in C loss when comparing internodes and nodes of bamboo aged 1–4 years. Moreover, Han et al. (2018) highlighted in their study that, in addition to aromaticity, ash content plays a role in enhancing the antioxidative properties of biochar. The differences in ash content observed among biochars derived at various pyrolysis temperatures and bamboo ages contribute to the variations in the antioxidative characteristics of biochar. In summary, this study demonstrated that temperature had a greater influence on chemical stability than

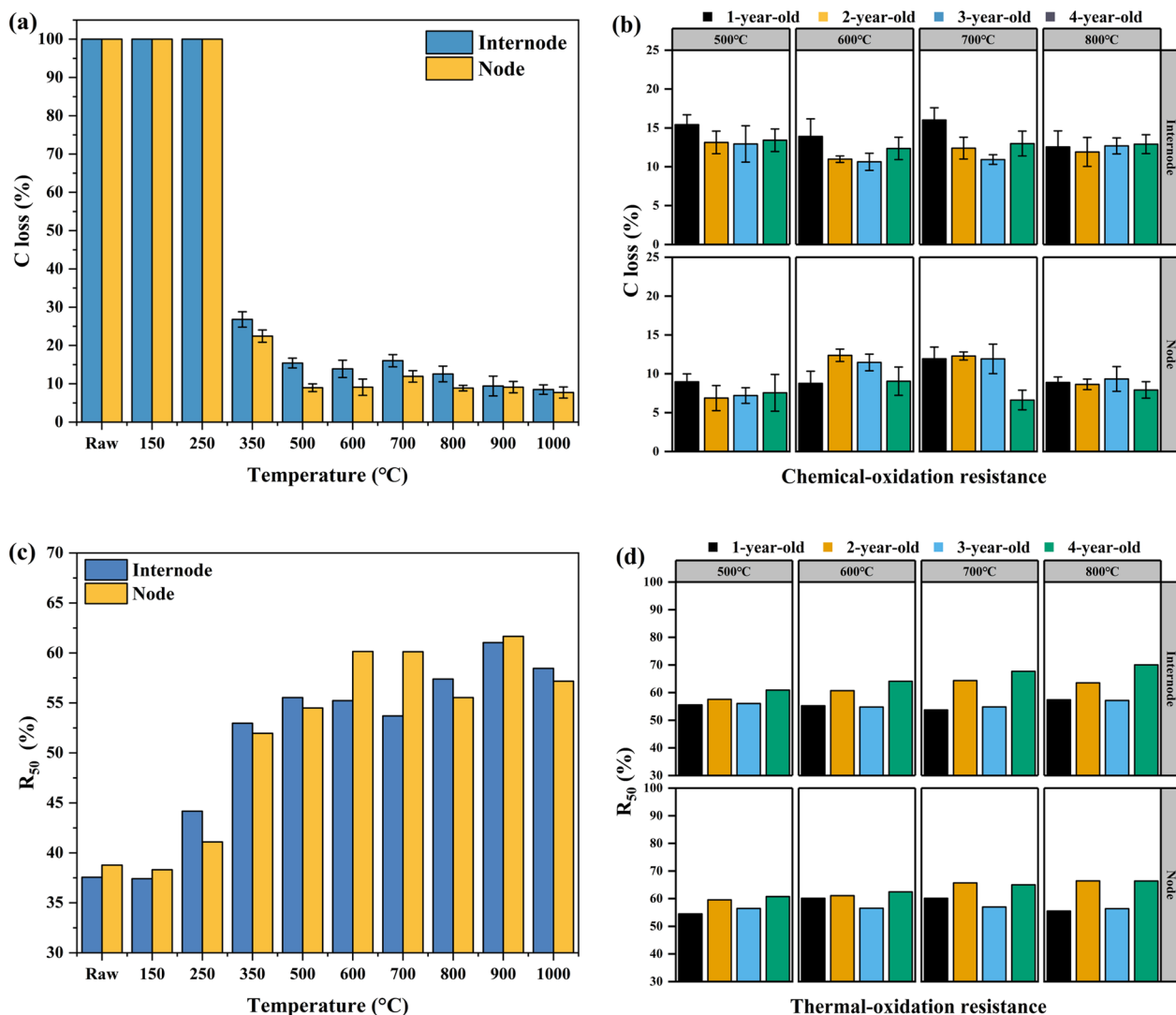


Fig. 4 Chemical-oxidation resistance of 1-year-old bamboo biochar (a). Chemical-oxidation resistance of biochar prepared from 1, 2, 3, and 4-year-old bamboo at the range of 500–800 °C (b). Thermal-oxidation resistance of 1-year-old bamboo biochar (c). Thermal-oxidation resistance of biochar prepared from 1, 2, 3, and 4-year-old bamboo at the range of 500–800 °C (d)

bamboo age, with minimal variations in C loss observed among internodes of bamboo aged 1–4 years and no significant differences among nodes. However, when comparing internodes and nodes of bamboo aged 1–4 years, nodes exhibited approximately 3% lower C loss than internodes, which could be attributed to the more intricate structural characteristics of nodes.

TGA was employed to assess the thermal oxidation stability (Harvey et al. 2012). The R_{50} values of bamboo and biochar were calculated using Eq. (2) with reference to graphite, and the results are presented in Fig. 4c and d. The bamboo treated below 350 °C exhibited lower R_{50} values, which were 37.56–44.17% for internodes and 38.77–41.09% for nodes. At lower temperatures,

the structures of cellulose, hemicelluloses, and lignin remained relatively intact, making them more susceptible to oxidation when exposed to air. However, as the temperature increased to 500 °C, the R_{50} values for internodes and nodes elevated to 55.34% and 54.50%, respectively. This increase in temperature favors the formation of stable carbon structures, thereby enhancing the carbon stability. However, with further temperature increase to above 500 °C, the biochar presented a relatively small increase in R_{50} values. When the temperature exceeded 800 °C, the R_{50} values of internodes ranged from 57.39% to 61.03%, while those of nodes were from 55.53% to 61.66%. The R_{50} values of biochar were similar to those reported in a recent study (Liu et al. 2020a).

Figure 4d illustrates the thermal oxidation stability of bamboo internodes and nodes of varying ages at 500–800 °C. At 500 °C, the R_{50} values of biochar obtained from 1-year-old internodes and nodes were 55.53% and 54.50%, respectively. In contrast, the R_{50} values of internodes from bamboo aged 2, 3, and 4 years increased by 2.04, 1.51, and 5.37, respectively, while those of nodes increased by 5.06, 1.96, and 6.27, respectively. Therefore, it can be inferred that the R_{50} value of biochar demonstrates a changing trend accordingly with the increase in bamboo age. As the temperature increased to 800 °C, the R_{50} values of biochar also experienced corresponding increases. Specifically, the R_{50} values for internodes and nodes from 1-year-old bamboo were 57.39% and 55.53%, respectively. And those for internodes from 2 and 4-year-old bamboo increased by 6.12% and 12.65%, respectively. Similarly, the R_{50} values for nodes from 2 and 4-year-old bamboo were elevated by 10.89% and 10.85%, respectively. It suggests that the R_{50} values possess a corresponding rise with an increase in bamboo age overall. However, there existed no remarkable difference in R_{50} values for internodes and nodes from 3-year-old bamboo compared to 1-year-old bamboo. Indeed, at the same temperature, the increase in bamboo age also affects the R_{50} values of biochar. This indicates that the thermal stability of biochar is influenced not only by the pyrolysis temperature but also by the bamboo age. However, this augment of thermal stability is not always linear.

Based on different stabilities determined by the TG analysis, carbon speciation can be divided into the following species (Fig. 5 and Additional file 1: Fig. S2): volatile organic-C (degradation range of 30–200 °C), labile organic-C (including cellulose, aliphatic-C, and carbohydrates, with a degradation range of 200–380 °C), recalcitrant organic-C (comprising lignin and aromatic C, with a degradation range of 380–475 °C), refractory organic-C (consisting of poly-condensed forms of lipids and

aromatic-C, with a degradation range of 475–600 °C), and inorganic-C (comprising elemental-C and carbonate, with a degradation range of 600–1000 °C) (Leng et al. 2019; Leng and Huang 2018).

Figure 5a illustrates that the primary composition of the bamboo was labile organic-C. As the pyrolysis temperature increased, there was a gradual reduction in the content of labile organic-C, accompanied by significant increment in contents of recalcitrant organic-C, refractory organic-C, and inorganic-C. This phenomenon can be attributed to the conversion of certain alkali and alkaline earth metals present in the bamboo material during the pyrolysis. At temperatures of 600 °C and 700 °C, the contents of recalcitrant organic-C, refractory organic-C, and inorganic-C in nodes were notably higher in comparison to those in internodes. This observation can explain the higher R_{50} values (Fig. 4c) in nodes compared to internodes at these two temperatures. Figure 5b and c explicates that, at the same pyrolysis temperature, the contents of recalcitrant organic-C, refractory organic-C, and inorganic-C became more with increasing bamboo age. This trend was consistent between internodes and nodes, supporting the observed increase in R_{50} values (Fig. 4d) with increasing bamboo age at the same pyrolysis temperature.

3.4 Morphological analysis

Figure 6a–j present the SEM images of a series of bamboo biochars obtained at various pyrolysis temperatures. Unlike the raw bamboo with intact cellular structures and a distinct fibrous texture (Fig. 6a), a series of changes occurred as the temperature increased from 150 °C to 350 °C. The cell walls gradually shrank and intercellular spaces enlarged, primarily due to the dehydration reaction with the increase in temperature. At 500 °C, the cellulose and hemicelluloses were decomposed completely,

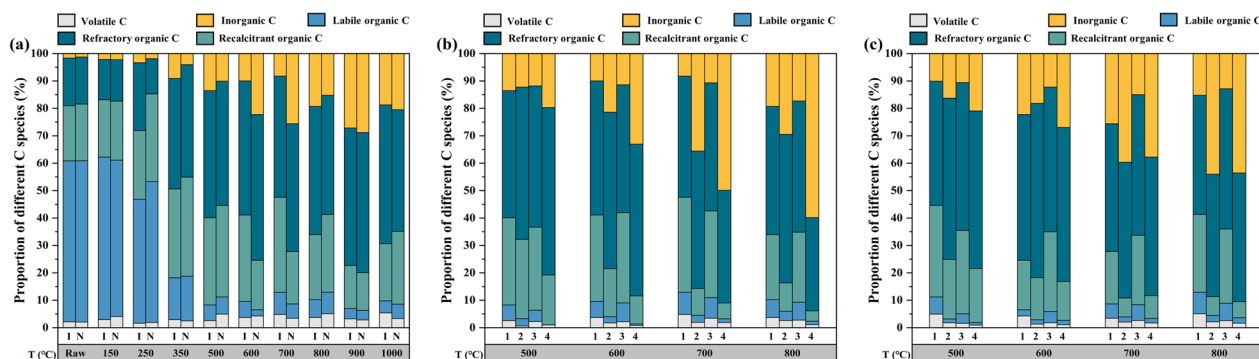


Fig. 5 Carbon proportion of biochar produced from different pyrolysis temperatures: internodes and nodes of 1-year-old bamboo (a); internodes of 1, 2, 3, and 4-year-old bamboo (b); nodes of 1, 2, 3, and 4-year-old bamboo (c)

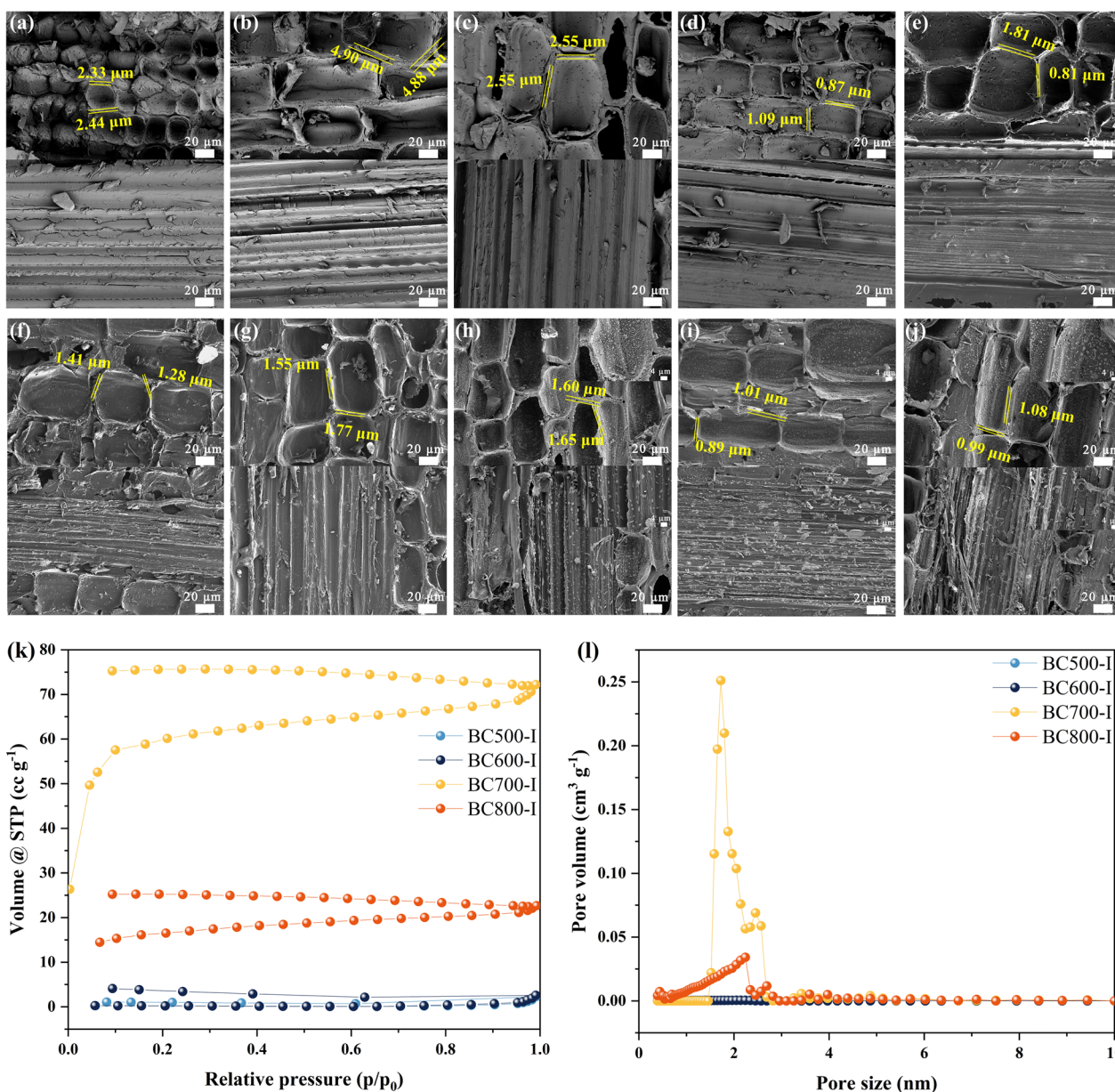


Fig. 6 The SEM of internode of 1-year-old bamboo: raw bamboo (a); bamboo biochar prepared at 150–1000 °C (b–j). The adsorption/desorption isotherms (k) and pore size distribution of biochar produced at temperatures ranging from 500 to 800 °C (l)

leading to thinner cell walls, smoother cell lumens, and a reduction in intercellular spacing (Fig. 6e). At 800 °C, the resulting biochar exhibited numerous crystals on the cell lumens and fiber surfaces, which were confirmed as potassium salts through energy dispersive spectroscopy (EDS) analysis (Additional file 1: Fig. S3).

In addition, the pyrolysis temperature influenced the pore structure of biochars. Figure 6l presents the N₂ adsorption/desorption isotherm of biochar produced at 500–800 °C. As pyrolysis was started, porous structures

emerged on the biochar surface due to the release of VM, resulting in visible pores and cracks. The biochar generated at 500 °C and 600 °C possessed relatively low surface areas of 0.62 m² g⁻¹ and 0.58 m² g⁻¹ (N₂ adsorption at 77 K), respectively, as outlined in Additional file 1: Table S2. Notably, it increased sharply to 217.21 m² g⁻¹ at 700 °C. This remarkable rise in specific surface area is primarily due to the release of volatile gases during the pyrolysis. As exhibited in Fig. 2d–g, the contents of CO₂ continuously increased for cellulose, hemicelluloses, and

lignin during the pyrolysis. Moreover, CO₂ exhibited an activation effect at higher temperatures, further enlarging the specific surface area of the biochar. However, the specific surface area of biochar produced at 800 °C experienced a notable decline, with a final value of 61.89 m² g⁻¹. This reduction can be attributed to the potential blockage of pores caused by ash crystals or the collapse of the carbon matrix due to excessively high temperatures. Yang et al. (2021) also indicated in their research that excessively high pyrolysis temperatures could potentially melt and damage the surface and pore structure of biochar, resulting in a reduction in specific surface area.

3.5 Crystals and graphitic structures of biochar

The degree of graphitization can be determined by observing the stacking of graphitic basal planes in the low-angle region [(002) peak] and the radial spread of crystalline structures in the high-angle region [(100) peak]. As given in Fig. 7a, b, the crystalline structure of biochar was greatly different from that of the raw materials. Specifically, the internodes and nodes of untreated bamboo showed at 16° and 22°. However, these two diffraction peaks displayed obviously decreased intensity with increasing pyrolysis temperature and were gradually transformed into one broad diffraction peak ranging from 15° to 30°. This indicates that the crystalline phase of cellulose is destroyed by high-temperature pyrolysis and gradually degrades. Pyrolysis temperatures above 300 °C led to the efficient destruction of the biomass structure. There were several broad (002) (JCPDS 89–8487) peaks centered around 26° with similar amplitude for the biochars generated above 500 °C, indicating that their structures were highly disordered. The characteristic diffraction peak at around 43° corresponded to the (100) (JCPDS 89–8487) and the (020) (JCPDS 74–2330) diffraction peak of the graphite structure. However, biochar obtained from 1-year-old bamboo did not present any distinct characteristic peak in this region. These findings aligned with the observations based on the TEM analysis. The highly corrugated graphite-like planes are clearly visible in Fig. 7e, which were typical characteristics of turbostratic chars dominated by disordered graphitic crystallites (Morstein et al. 2022; Toth 2021; Wei et al. 2022).

However, biochar derived from 2, 3, and 4-year-old bamboo exhibited a distinct peak around 43°. As explained in Fig. 7c, the graphite peak showed a gradually increased intensity and became sharper with increasing temperature, indicative of the presence of graphitic structures. HR-TEM analysis, as depicted in Fig. 7f–h, revealed a favorable crystallinity of biochars derived from 2, 3, and 4-year-old bamboo at 800 °C. The interlayer spacing of biochar from 2 and 4-year-old bamboo

measured 0.219 nm and 0.253 nm at 800 °C, respectively, aligning with the interlayer spacing of the (100) (Li et al. 2018b; Zhang et al. 2022c,) and (020) (Chen et al. 2018, 2021) plane in graphite carbon, respectively. Furthermore, biochar from 3-year-old bamboo at 800 °C displayed a lattice spacing of 0.341 nm. The XRD spectrum suggested a broad peak around 23° (Fig. 7c), indicative of the presence of the (002) (Liu et al. 2022; Zhang et al. 2023; Zhao et al. 2022) plane of graphite carbon and suggesting a layered structure. Therefore, 800 °C is a critical temperature point in preparing biochar with a graphitic structure.

The graphitization and crystal structure of the carbon materials were further studied through Raman spectroscopy analysis. The I_D/I_G ratio can reflect the degree of disorder degree and defect density of the sample, with lower values indicating a higher degree of graphitization (Ma et al. 2017; Tong et al. 2020). As elucidated in Fig. 7d, the Raman intensity of biochar obtained at varying temperatures exhibited distinctive patterns. Specifically, for biochar originating from 1-year-old bamboo, the I_D/I_G ratios were measured at 2.80 for internodes and 2.99 for nodes when pyrolyzed at 500 °C. As the temperature was elevated to 800 °C, the I_D/I_G ratios for internodes and nodes increased to 3.41 and 3.40, respectively. This shift suggests a higher proportion of sp² structures and an increase in biochar defects. At 1000 °C, the I_D/I_G ratios of biochar obtained from 1-year-old bamboo decreased to 2.85 for internodes and 2.60 for nodes, indicating the promotive role of higher temperatures in enhancing the ordered structure of biochar. Remarkably, there was no significant difference in the I_D/I_G ratios between internodes and nodes, and both exhibited similar trends in I_D/I_G changes with increasing temperature.

Figure 7d illustrates the I_D/I_G ratios of biochar from 2 to 4-year-old bamboo internodes and nodes at 500–800 °C. At 500 °C, the I_D/I_G ratio for biochar originating from internodes aged 2–4 years ranged from 2.73 to 3.06, while that for biochar from nodes was within the range of 2.58 to 2.79. Generally, biochar obtained from nodes exhibited lower I_D/I_G ratios than that from internodes, implying a greater degree of structural order during the biochar preparation from nodes compared to internodes. As the temperature was increased to 800 °C, the I_D/I_G ratios of biochar prepared from internodes of bamboo of aged 2, 3, and 4 years increased to 2.82–3.21, while that of biochar from nodes increased to 2.86–3.74. These results indicate that with the increase in temperature, the I_D/I_G ratios of biochar prepared from bamboo of varying ages also increase accordingly, which may be attributed to pore shrinkage, leading to a less ordered structure. Furthermore,

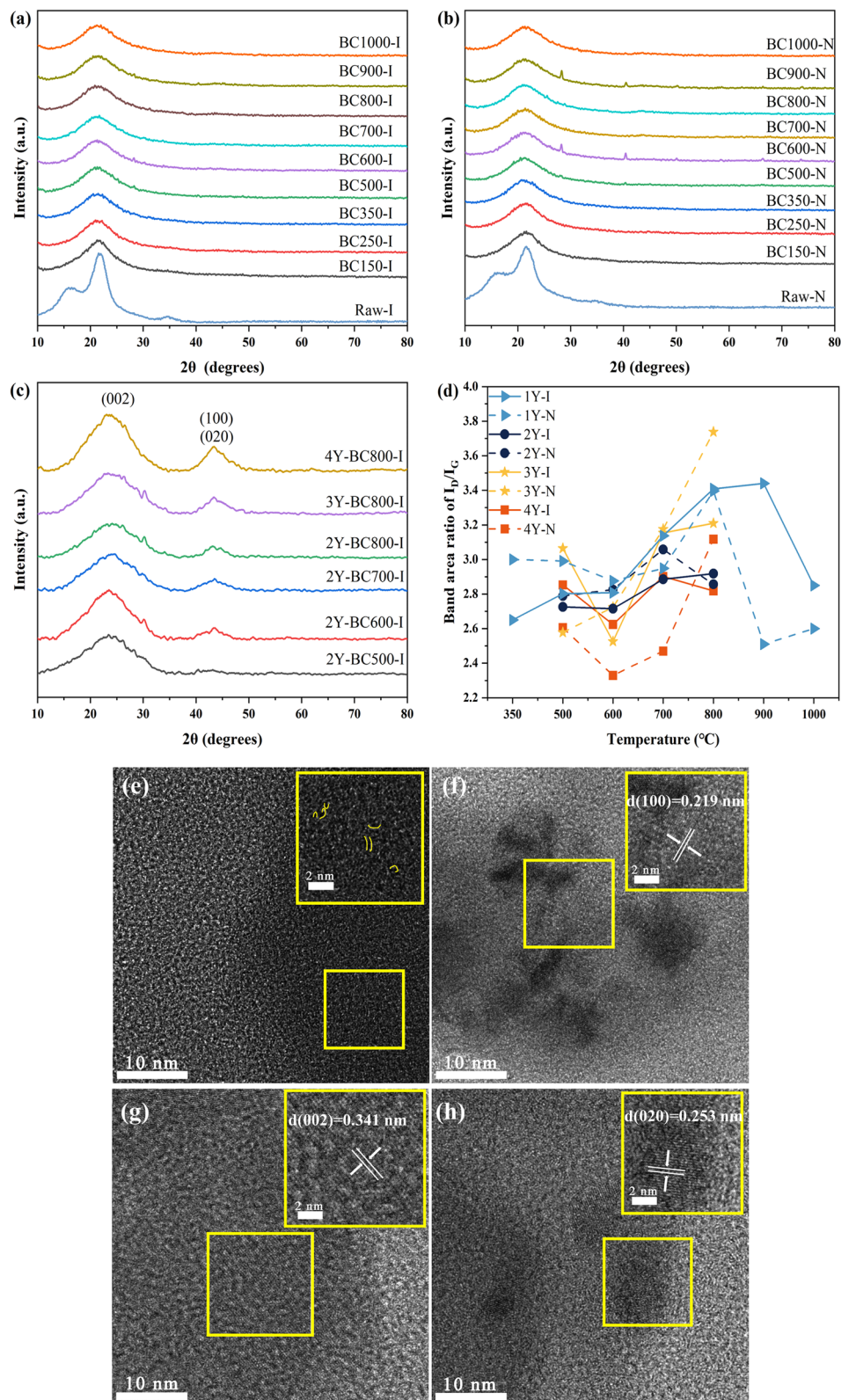


Fig. 7 X-Ray diffraction results for different ages of bamboo internodes and nodes: internodes (a) and nodes (b) of 1-year-old; internode of 2, 3, and 4-year-old (c); the effect of temperature on the ratio of D band and G band (d). TEM image of biochar produced at 800 °C: 1-year-old (e); 2-year-old (f); 3-year-old (g); 4-year-old (h)

the increase in bamboo age was also associated with elevated I_D/I_G ratios in the resulting biochar, indicating that bamboo age also influences the degree of structural ordering in the biochar.

3.6 Decisive factors for biochar physicochemical properties

To comprehensively assess the impacts of pyrolysis temperature, bamboo age, and different bamboo parts on the physicochemical properties of biochar, the PCC was utilized to evaluate their correlations (Fig. 8 and Additional file 1: Table S3). Various basic properties of biochar were considered, including proximate analysis of biochars, H/C, O/C, (N + O)/C, AI, C–C/C=C/C–H, and different carbon types of ratios based on the TG analysis. The R_{50} values and C loss were selected to assess the resistance to thermal oxidation and chemical stability, respectively.

The results revealed that pyrolysis temperature exhibited significant positive correlations ($p < 0.01$) with ash content (0.76), FC (0.97), AI (0.81), R_{50} value (0.77), C–C/C=C/C–H functional groups (0.87), refractory organic-C (0.62), and inorganic-C (0.62). Furthermore, significant negative correlations ($p < 0.01$) were observed with VM (–0.91), O/C ratio (0.88), H/C ratio (–0.95), (N + O)/C ratio (–0.87), C loss (–0.79), and labile organic-C (–0.78). Additionally, a remarkable negative association was found with recalcitrant organic-C (–0.31, $p < 0.05$). This confirmed that with an increase in pyrolysis temperature, the volatilization of organic components in biochar leads to an increase in carbon content and ash content. Additionally, there was an increase in the content of aromatic carbon from recalcitrant organic-C or inorganic-C with high thermal stability. This enhances the thermal oxidation resistance stability of the biochar, consequently

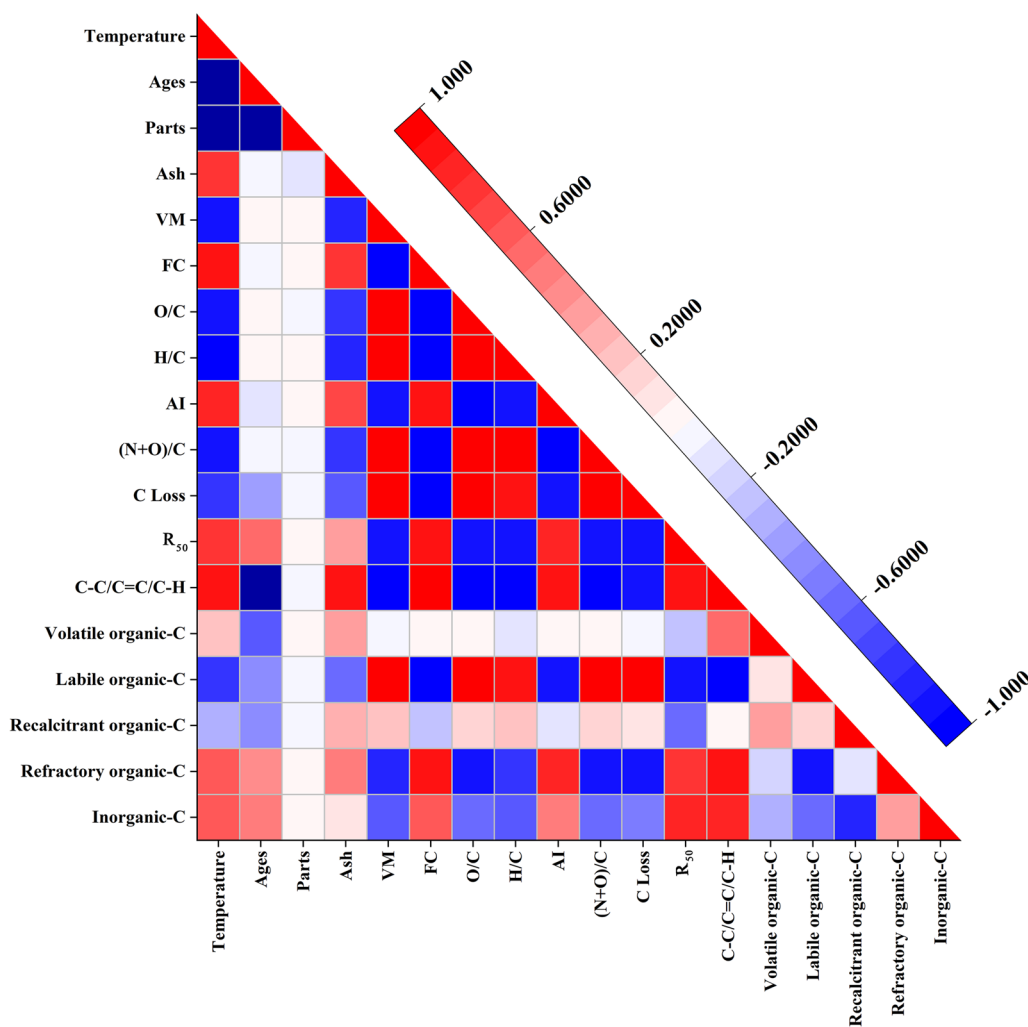


Fig. 8 Pearson correlation matrix

reducing the C loss rate. The bamboo age was negatively correlated ($p < 0.01$) with C loss (-0.40), volatile organic-C (-0.63), labile organic-C (-0.45), and recalcitrant organic-C (-0.40). Conversely, it exhibited significant positive correlations ($p < 0.01$) with R_{50} (0.54), refractory organic-C (0.42), and inorganic-C (0.52). The aforementioned correlations can be attributed to variations in ash content, cellulose, hemicelluloses, and lignin content among bamboo samples of different ages (Hossain et al. 2022; Sadiku et al. 2016; Wang et al. 2016). However, no obvious association was observed between the parts (internodes and nodes) of bamboo and the physicochemical properties of biochars.

4 Conclusion

This study evaluated the impacts of pyrolysis temperature on the physicochemical properties of bamboo biochar. The findings highlighted the critical turning points at 500 °C and 800 °C. At 150–500 °C, elevating the temperature resulted in decreased contents of H and O, while increasing the C content in the biochar. At 500–1000 °C, the decrease rates in contents of H and O slowed down, and notably, a graphite-like structure was observed at 800 °C. Furthermore, bamboo age significantly influenced the chemical and thermal stability of the biochar. Specifically, as bamboo age increased, the biochar exhibited enhanced chemical and thermal stability, accompanied by changes in the proportion of different carbon types.

On the other hand, different parts of the bamboo (internodes and nodes) did not exert a noticeable influence on the physicochemical properties of the biochar. The findings highlighted the significant effects of temperature and bamboo age on the physicochemical attributes of bamboo biochar. This insight provided valuable guidance for the targeted production and utilization of bamboo biochar in various fields such as water treatment, soil carbon sequestration, and energy storage.

Supplementary Information

The online version contains supplementary material available at <https://doi.org/10.1007/s42773-024-00321-6>.

Additional file 1: Table S1. The cellulose, hemicelluloses, and lignin content of *moso* bamboo at different ages. **Table S2.** Specific surface area of biochar. **Table S3.** Pearson correlation coefficient analysis results of biochar (** $p < 0.01$, * $p < 0.05$). **Figure S1.** The content of $C-C/C=C/C-H$ determined by spectra C 1s of XPS. **Figure S2.** TG and DTG curves of biochar with different pyrolysis temperatures: internode (a, b) and node (c, d) of 1-year-old bamboo; bamboo of 2-year-old (e, f); bamboo of 3-year-old (g, h); bamboo of 4-year-old (i, j). **Figure S3.** Energy dispersive spectrometer (EDS) analysis of biochar produced at 800 °C.

Acknowledgements

The authors are grateful for grants from the Fundamental Research Funds of ICBR (Grant No 1632022008) and the National Key R&D Program of China (2022YFD2200904).

Author contributions

JW (Jiajun Wang): conceptualization, sampling, analysis, visualization, writing original draft and review. ZL (Zhenrui Li): sampling, analysis and investigation. YL (Yujun Li): sampling, analysis and investigation. ZW (Zhihui Wang): sampling and investigation. XL (Xing'e Liu): analysis, review, editing and supervision. ZL (Zhenzhen Liu): review and supervision. JM (Jianfeng Ma): review, editing, supervision, project administration and funding acquisition. All authors read and approved the final manuscript.

Funding

The authors are grateful for grants from the Fundamental Research Funds of ICBR (Grant No 1632022008) and the National Key R&D Program of China (2022YFD2200904).

Availability of data and materials

All data generated or analyzed during this study are included in this published article and its Additional information files.

Declarations

Competing interests

All authors declare no competing interest.

Author details

¹Key Lab of Bamboo and Rattan Science & Technology, International Center for Bamboo and Rattan, Beijing 100102, China.

Received: 24 September 2023 Revised: 6 March 2024 Accepted: 10 March 2024

Published online: 28 March 2024

References

- Ávila PF, Forte MB, Goldbeck R (2018) Evaluation of the chemical composition of a mixture of sugarcane bagasse and straw after different pretreatments and their effects on commercial enzyme combinations for the production of fermentable sugars. *Biomass Bioenerg* 116:180–188. <https://doi.org/10.1016/j.biombioe.2018.06.015>
- Cayuela ML, Jeffery S, Van Zwieten L (2015) The molar H: Corg ratio of biochar is a key factor in mitigating N₂O emissions from soil. *Agric Ecosyst Environ* 202:135–138. <https://doi.org/10.1016/j.agee.2014.12.015>
- Chen D, Yu X, Song C, Pang X, Huang J, Li Y (2016) Effect of pyrolysis temperature on the chemical oxidation stability of bamboo biochar. *Bioresour Technol* 218:1303–1306. <https://doi.org/10.1016/j.biortech.2016.07.112>
- Chen W, Li D, Tian L, Xiang W, Wang T, Hu W, Hu Y, Chen S, Chen J, Dai Z (2018) Synthesis of graphene quantum dots from natural polymer starch for cell imaging. *Green Chem* 20:4438–4442. <https://doi.org/10.1039/c8gc02106f>
- Chen S, Wang J, Xia L, Wu Y (2019) Deformation behavior of bulk metallic glasses and high entropy alloys under complex stress fields: a review. *Entropy* 21:54. <https://doi.org/10.3390/e21010054>
- Chen W, Shen J, Wang Z, Liu X, Xu Y, Zhao H, Astruc D (2021) Turning waste into wealth: facile and green synthesis of carbon nanodots from pollutants and applications to bioimaging. *Chem Sci* 12:11722–11729. <https://doi.org/10.1039/d1sc02837e>
- Chen D, Cen K, Zhuang X, Gan Z, Zhou J, Zhang Y, Zhang H (2022) Insight into biomass pyrolysis mechanism based on cellulose, hemicellulose, and lignin: evolution of volatiles and kinetics, elucidation of reaction pathways, and characterization of gas, biochar and bio-oil. *Combust Flame* 242:112142. <https://doi.org/10.1016/j.combustflame.2022.112142>
- Cheng L, Adhikari S, Wang Z, Ding Y (2015) Characterization of bamboo species at different ages and bio-oil production. *J Anal Appl Pyrol* 116:215–222. <https://doi.org/10.1016/j.jaap.2015.09.008>
- Chu G, Zhao J, Liu Y, Lang D, Wu M, Pan B, Steinberg CEW (2019) The relative importance of different carbon structures in biochars to carbamazepine

- and bisphenol A sorption. *J Hazard Mater* 373:106–114. <https://doi.org/10.1016/j.jhazmat.2019.03.078>
- de Almeida SG, Tarelho LA, Hauschild T, Costa MA, Dussán KJ (2022) Biochar production from sugarcane biomass using slow pyrolysis: characterization of the solid fraction. *Chem Eng Process* 179:109054. <https://doi.org/10.1016/j.cep.2022.109054>
- Dong J, Jiang P, Wang H, Lu R, Liu Y, Li Y, Gan Y, Bolan N (2023) Influence of biomass feedstocks on magnetic biochar preparation for efficient Pb(II) removal. *Environ Technol Innov* 32:103363. <https://doi.org/10.1016/j.eti.2023.103363>
- Fan J, Duan T, Zou L, Sun J (2023) Characteristics of dissolved organic matter composition in biochar: effects of feedstocks and pyrolysis temperatures. *Environ Sci Pollut R* 30:85139–85153. <https://doi.org/10.1007/s11356-023-28431-x>
- Gabhi R, Basile L, Kirk DW, Giorelli M, Tagliaferro A, Jia CQ (2020) Electrical conductivity of wood biochar monoliths and its dependence on pyrolysis temperature. *Biochar*. 2:369–378. <https://doi.org/10.1007/s42773-020-00056-0>
- Gupta S, Gupta GK, Mondal MK (2019) Slow pyrolysis of chemically treated walnut shell for valuable products: effect of process parameters and in-depth product analysis. *Energy* 181:665–676. <https://doi.org/10.1016/j.energy.2019.05.214>
- Han L, Ro KS, Wang Y, Sun K, Sun H, Libra JA, Xing B (2018) Oxidation resistance of biochars as a function of feedstock and pyrolysis condition. *Sci Total Environ* 616:335–344. <https://doi.org/10.1016/j.scitotenv.2017.11.014>
- Han L, Sun K, Yang Y, Xia X, Li F, Yang Z, Xing B (2020) Biochar's stability and effect on the content, composition and turnover of soil organic carbon. *Geoderma* 364:114184. <https://doi.org/10.1016/j.geoderma.2020.114184>
- Harvey OR, Kuo L-J, Zimmerman AR, Louchouart P, Amonette JE, Herbert BE (2012) An index-based approach to assessing recalcitrance and soil carbon sequestration potential of engineered black carbons (Biochars). *Environ Sci Technol* 46:1415–1421. <https://doi.org/10.1021/es2040398>
- Hien TTT, Tsubota T, Taniguchi T, Shinogi Y (2020) Enhancing soil water holding capacity and provision of a potassium source via optimization of the pyrolysis of bamboo biochar. *Biochar*. 3:51–61. <https://doi.org/10.1007/s42773-020-00071-1>
- Hossain MJ, Ghosh RK, Das AK, Maryana R, Nath SC, Islam MR, Sarker SC (2022) Effect of age and height on the chemical properties of muli bamboo (*Melocanna baccifera*). *ACS Omega* 7:39370–39374. <https://doi.org/10.1021/acsomega.2c05684>
- Hou Y, Liang Y, Hu H, Tao Y, Zhou J, Cai J (2021) Facile preparation of multiporous biochar from lotus biomass for methyl orange removal: Kinetics, isotherms, and regeneration studies. *Bioresour Technol* 329:124877. <https://doi.org/10.1016/j.biortech.2021.124877>
- Iroegbu A, Ray S (2021) Bamboos: from bioresource to sustainable materials and chemicals. *Sustainability* 13:12200. <https://doi.org/10.3390/su132112200>
- Kearns JP, Wellborn LS, Summers RS, Knappe DRU (2014) 2,4-D adsorption to biochars: Effect of preparation conditions on equilibrium adsorption capacity and comparison with commercial activated carbon literature data. *Water Res* 62:20–28. <https://doi.org/10.1016/j.watres.2014.05.023>
- Keilweil M, Nico PS, Johnson MG, Kleber M (2010) Dynamic molecular structure of plant biomass-derived black carbon (biochar). *Environ Sci Technol* 44:1247–1253. <https://doi.org/10.1021/es9031419>
- Kim KH, Kim JY, Cho TS, Choi JW (2012) Influence of pyrolysis temperature on physicochemical properties of biochar obtained from the fast pyrolysis of pitch pine (*Pinus rigida*). *Bioresour Technol* 118:158–162. <https://doi.org/10.1016/j.biortech.2012.04.094>
- Leng L, Huang H (2018) An overview of the effect of pyrolysis process parameters on biochar stability. *Bioresour Technol* 270:627–642. <https://doi.org/10.1016/j.biortech.2018.09.030>
- Leng L, Huang H, Li H, Li J, Zhou W (2019) Biochar stability assessment methods: a review. *Sci Total Environ* 647:210–222. <https://doi.org/10.1016/j.scitotenv.2018.07.402>
- Li Z, Zeng Q, Wu Z, Zhou G, Chen B (1998) Estimation of amount of carbon pool in natural tropical forest of China. *For Res* 2:41–47. <https://doi.org/10.13275/j.cnki.lykxyj.1998.02.008>
- Li H, Dong X, Da Silva EB, De Oliveira LM, Chen Y, Ma LQ (2017) Mechanisms of metal sorption by biochars: biochar characteristics and modifications. *Chemosphere* 178:466–478. <https://doi.org/10.1016/j.chemosphere.2017.03.072>
- Li C, Shi Y, Zhou G, Zhou Y, Xu L, Tong L, Liu X (2018a) Effects of different management approaches on soil carbon dynamics in moso bamboo forest ecosystems. *Catena* 169:59–68. <https://doi.org/10.1016/j.catena.2018.05.031>
- Li W, Liu Y, Wu M, Feng X, Redfern SA, Shang Y, Yong X, Feng T, Wu K, Liu Z, Li B (2018b) Carbon-quantum-dots-loaded ruthenium nanoparticles as an efficient electrocatalyst for hydrogen production in alkaline media. *Adv Mater* 30:e1800676. <https://doi.org/10.1002/adma.201800676>
- Lian W, Shi W, Tian S, Gong X, Yu Q, Lu H, Liu Z, Zheng J, Wang Y, Bian R, Li L, Pan G (2023) Preparation and application of biochar from co-pyrolysis of different feedstocks for immobilization of heavy metals in contaminated soil. *Waste Manage* 163:12–21. <https://doi.org/10.1016/j.wasman.2023.03.022>
- Liang F, Wang R, Hongzhong X, Yang X, Zhang T, Hu W, Mi B, Liu Z (2018) Investigating pyrolysis characteristics of moso bamboo through TG-FTIR and Py-GC/MS. *Bioresour Technol* 256:53–60. <https://doi.org/10.1016/j.biortech.2018.01.140>
- Liu G, Pan X, Ma X, Xin S, Xin Y (2020a) Effects of feedstock and inherent mineral components on oxidation resistance of biochars. *Sci Total Environ* 726:138672. <https://doi.org/10.1016/j.scitotenv.2020.138672>
- Liu Y, Gao C, Wang Y, He L, Lu H, Yang S (2020b) Vermiculite modification increases carbon retention and stability of rice straw biochar at different carbonization temperatures. *J Clean pro* 254:120111. <https://doi.org/10.1016/j.jclepro.2020.120111>
- Liu X, Wang T, Zhang T, Sun Z, Ji T, Tian J, Wang H, Hao X, Liu H, Chao D (2022) Solvated sodium storage via a coadsorptive mechanism in microcrystalline graphite fiber. *Adv Energy Mater* 12:2202388. <https://doi.org/10.1002/aenm.202202388>
- Ma Z, Yang Y, Ma Q, Zhou H, Luo X, Liu X, Wang S (2017) Evolution of the chemical composition, functional group, pore structure and crystallographic structure of bio-char from palm kernel shell pyrolysis under different temperatures. *J Anal Appl Pyrol* 127:350–359. <https://doi.org/10.1016/j.jaap.2017.07.015>
- Meier S, Curaqueo G, Khan N, Bolan N, Cea M, Eugenia GM, Cornejo P, Ok YS, Borie F (2015) Chicken-manure-derived biochar reduced bioavailability of copper in a contaminated soil. *J Soil Sediment*. 17:741–750. <https://doi.org/10.1007/s11368-015-1256-6>
- Morstein CE, Klemenz A, Dienwiebel M, Moseler M (2022) Humidity-dependent lubrication of highly loaded contacts by graphite and a structural transition to turbostratic carbon. *Nat Commun* 13:5958. <https://doi.org/10.1038/s41467-022-33481-9>
- Mu L, Wang R, Xie P, Li Y, Huang X, Yin H, Dong M (2023) Comparative investigation on the pyrolysis of crop, woody, and herbaceous biomass: Pyrolytic products, structural characteristics, and CO₂ gasification. *Fuel* 335:126940. <https://doi.org/10.1016/j.fuel.2022.126940>
- Nan H, Zhao L, Yang F, Liu Y, Xiao Z, Cao X, Qiu H (2020) Different alkaline minerals interacted with biomass carbon during pyrolysis: Which one improved biochar carbon sequestration. *J Clean pro* 255:120162. <https://doi.org/10.1016/j.jclepro.2020.120162>
- Nan H, Yin J, Yang F, Luo Y, Zhao L, Cao X (2021) Pyrolysis temperature-dependent carbon retention and stability of biochar with participation of calcium: Implications to carbon sequestration. *Environ Pollut*. <https://doi.org/10.1016/j.envpol.2021.117566>
- Nanda S, Dalai AK, Berruti F, Kozinski JA (2015) Biochar as an exceptional bioresource for energy, agronomy, carbon sequestration, activated carbon and specialty materials. *Waste Biomass Valoriz*. 7:201–235. <https://doi.org/10.1007/s12649-015-9459-z>
- Nath AJ, Lal R, Das AK (2015) Managing woody bamboos for carbon farming and carbon trading. *Glob Ecol Conserv*. 3:654–663. <https://doi.org/10.1016/j.gecco.2015.03.002>
- Pradhan S, Abdelaal AH, Mroue K, Al-Ansari T, Mackey HR, Mckay G (2020) Biochar from vegetable wastes: agro-environmental characterization. *Biochar*. 2:439–453. <https://doi.org/10.1007/s42773-020-00069-9>
- Rodier L, Bilba K, Onésippe C, Arsène MA (2019) Utilization of bio-chars from sugarcane bagasse pyrolysis in cement-based composites. *Ind Crop Prod* 141:111731. <https://doi.org/10.1016/j.indcrop.2019.111731>
- Ruan H, Jiang Z, Gao S (1997) Preliminary studies of carbon cycling in three types of forests in the hilly regions of southern Jiangsu Province. *Chin J Ecol* 16(6):17–21. <https://doi.org/10.13292/j.1000-4890.1997.0088>

- Sadiku NA, Oluyeye AO, Ajayi B (2016) Fibre dimension and chemical characterisation of naturally grown *Bambusa vulgaris* for pulp and paper production. *J Bamboo Ratta*. 15:33–43
- Sahoo SS, Vijay VK, Chandra R, Kumar H (2021) Production and characterization of biochar produced from slow pyrolysis of pigeon pea stalk and bamboo. *Clean Eng Technol*. 3:100101. <https://doi.org/10.1016/j.clet.2021.100101>
- Selvarajoo A, Wong YL, Khoo KS, Chen W-H, Show PL (2022) Biochar production via pyrolysis of citrus peel fruit waste as a potential usage as solid biofuel. *Chemosphere* 294:133671. <https://doi.org/10.1016/j.chemosphere.2022.133671>
- Shaheen SM, Niazi NK, Hassan NEE, Bibi I, Wang H, Tsang Daniel CW, Ok YS, Bolan N, Rinklebe J (2018) Wood-based biochar for the removal of potentially toxic elements in water and wastewater: a critical review. *Int Mater Rev* 64:216–247. <https://doi.org/10.1080/09506608.2018.1473096>
- Shimabuku KK, Kearns JP, Martinez JE, Mahoney RB, Moreno-Vasquez L, Summers RS (2016) Biochar sorbents for sulfamethoxazole removal from surface water, stormwater, and wastewater effluent. *Water Res* 96:236–245. <https://doi.org/10.1016/j.watres.2016.03.049>
- Sun K, Kang M, Ro KS, Libra JA, Zhao Y, Xing B (2016) Variation in sorption of propiconazole with biochars: the effect of temperature, mineral, molecular structure, and nano-porosity. *Chemosphere* 142:56–63. <https://doi.org/10.1016/j.chemosphere.2015.07.018>
- Suthar R, Wang C, Nunes M, Chen J, Sargent S, Bucklin R, Gao B (2018) Bamboo biochar pyrolyzed at low temperature improves tomato plant growth and fruit quality. *Agriculture* 8:153. <https://doi.org/10.3390/agriculture8100153>
- Tan X, Liu Y, Zeng G, Wang X, Hu X, Gu Y, Yang Z (2015) Application of biochar for the removal of pollutants from aqueous solutions. *Chemosphere* 125:70–85. <https://doi.org/10.1016/j.chemosphere.2014.12.058>
- Tong W, Cai Z, Liu Q, Ren S, Kong M (2020) Effect of pyrolysis temperature on bamboo char combustion: reactivity, kinetics and thermodynamics. *Energy* 211:118736. <https://doi.org/10.1016/j.energy.2020.118736>
- Tonnoir H, Huo D, Davoisne C, Celzard A, Fierro V, Saurel D, El Marssi M, Benyoussef M, Meunier P, Janot R (2023) Pyrolysis temperature dependence of sodium storage mechanism in non-graphitizing carbons. *Carbon* 208:216–226. <https://doi.org/10.1016/j.carbon.2023.03.055>
- Toth P (2021) Nanostructure quantification of turbostratic carbon by HRTEM image analysis: state of the art, biases, sensitivity and best practices. *Carbon* 178:688–707. <https://doi.org/10.1016/j.carbon.2021.03.043>
- Ullah H, Abbas Q, Ali MU, Amina CAI, Yousaf B, Rinklebe J (2019) Synergistic effects of low-/medium-vacuum carbonization on physico-chemical properties and stability characteristics of biochars. *Chem Eng J* 373:44–57. <https://doi.org/10.1016/j.cej.2019.05.025>
- Viglašová E, Galamboš M, Danková Z, Krivosudský L, Lengauer CL, Hood-Nowotny R, Soja G, Rompel A, Matik M, Bričanin J (2018) Production, characterization and adsorption studies of bamboo-based biochar/montmorillonite composite for nitrate removal. *Waste Manage* 79:385–394. <https://doi.org/10.1016/j.wasman.2018.08.005>
- Wan J, Liu F, Wang G, Liang W, Peng C, Zhang W, Lin K, Yang J (2021) Exploring different mechanisms of biochars in removing hexavalent chromium: sorption, reduction and electron shuttle. *Bioresour Technol* 337:125382. <https://doi.org/10.1016/j.biortech.2021.125382>
- Wang J, Xiong Z, Kuzyakov Y (2015) Biochar stability in soil: meta-analysis of decomposition and priming effects. *Gcb Bioenergy*. 8:512–523. <https://doi.org/10.1111/gcbb.12266>
- Wang S, Lin S, Li W, Ding Y (2016) Variations in fiber morphology and chemical components of *dendrocalamus giganteus*. *Forest Prod J*. 66:319–325. <https://doi.org/10.13073/fpj-d-15-00043>
- Wang Z, Wang J, Xie L, Zhu H, Shu X (2019) Influence of the addition of cotton stalk during co-pyrolysis with sewage sludge on the properties, surface characteristics, and ecological risks of biochars. *J Therm Sci* 28:755–762. <https://doi.org/10.1007/s11630-019-1100-1>
- Wang Q, Chen Z, Luo Q, Li H, Li J, Yang W (2023a) Capillary evaporation on high-dense conductive ramie carbon for assisting highly volumetric-performance supercapacitors. *Small*. <https://doi.org/10.1002/smll.202303349>
- Wang Y, Yu G, Xie S, Jiang R, Li C, Xing Z (2023b) Pyrolysis of food waste digestate residues for biochar: pyrolytic properties, biochar characterization, and heavy metal behaviours. *Fuel* 353:129185. <https://doi.org/10.1016/j.fuel.2023.129185>
- Weber K, Quicker P (2018) Properties of biochar. *Fuel* 217:240–261. <https://doi.org/10.1016/j.fuel.2017.12.054>
- Wei L, Huang Y, Huang L, Li Y, Huang Q, Xu G, Müller K, Wang H, Ok YS, Liu Z (2020) The ratio of H/C is a useful parameter to predict adsorption of the herbicide metolachlor to biochars. *Environ Res* 184:109324. <https://doi.org/10.1016/j.envres.2020.109324>
- Wei X, Zhang W, Chen L, Xia X, Meng Y, Liu C, Lin Q, Jiang Y, Gao S (2022) Evaluation of graphitization and tensile property in microwave plasma treated carbon fiber. *Diam Relat Mater* 126:109094. <https://doi.org/10.1016/j.diamond.2022.109094>
- Weldon S, Rasse DP, Budai A, Tomic O, Dörsch P (2019) The effect of a biochar temperature series on denitrification: which biochar properties matter? *Soil Biol Biochem* 135:173–183. <https://doi.org/10.1016/j.soilbio.2019.04.018>
- Wu X, Ba Y, Wang X, Niu M, Fang K (2018) Evolved gas analysis and slow pyrolysis mechanism of bamboo by thermogravimetric analysis, fourier transform infrared spectroscopy and gas chromatography-mass spectrometry. *Bioresour Technol* 266:407–412. <https://doi.org/10.1016/j.biortech.2018.07.005>
- Xu L, Fang H, Deng X, Ying J, Lv W, Shi Y, Zhou G, Zhou Y (2020) Biochar application increased ecosystem carbon sequestration capacity in a moso bamboo forest. *For Ecol Manag* 475:118447. <https://doi.org/10.1016/j.foreco.2020.118447>
- Xu Z, He M, Xu X, Cao X, Tsang DCW (2021) Impacts of different activation processes on the carbon stability of biochar for oxidation resistance. *Bioresour Technol* 338:125555. <https://doi.org/10.1016/j.biortech.2021.125555>
- Yang F, Zhao L, Gao B, Xu X, Cao X (2016) The interfacial behavior between biochar and soil minerals and its effect on biochar stability. *Environ Sci Technol* 50:2264–2271. <https://doi.org/10.1021/acs.est.5b03656>
- Yang E, Yao C, Liu Y, Zhang C, Jia L, Li D, Fu Z, Sun D, Robert Kirk S, Yin D (2018) Bamboo-derived porous biochar for efficient adsorption removal of dibenzothiophene from model fuel. *Fuel* 211:121–129. <https://doi.org/10.1016/j.fuel.2017.07.099>
- Yang C, Liu J, Lu S (2021) Pyrolysis temperature affects pore characteristics of rice straw and canola stalk biochars and biochar-amended soils. *Geoderma*. <https://doi.org/10.1016/j.geoderma.2021.115097>
- Yen TM, Lee JS (2011) Comparing aboveground carbon sequestration between moso bamboo (*phyllostachys pubescens*) and China fir (*Cunninghamia lanceolata*) forests based on the allometric model. *For Ecol Manag* 261:995–1002. <https://doi.org/10.1016/j.foreco.2010.12.015>
- Zeng L, Hu X, Gu N, Fu B, Qin C (2015) Investigation of volatile chemicals and their distributions from pyrolysis of chitin by FT-IR and GC-MS. *J Anal Appl Pyrol* 112:357–362. <https://doi.org/10.1016/j.jaap.2014.12.026>
- Zhang Y, Ma Z, Zhang Q, Wang J, Ma Q, Yang Y, Luo X, Zhang W (2017) Comparison of the physicochemical characteristics of bio-char pyrolyzed from moso bamboo and rice husk with different pyrolysis temperatures. *Bioresour* 12(3):4652–4669. <https://doi.org/10.15376/biores.12.3.4652-4669>
- Zhang C, Zhang L, Gao J, Zhang S, Liu Q, Duan P, Hu X (2020a) Evolution of the functional groups/structures of biochar and heteroatoms during the pyrolysis of seaweed. *Algal Res* 48:101900. <https://doi.org/10.1016/j.algal.2020.101900>
- Zhang C, Zhang Z, Zhang L, Li Q, Li C, Chen G, Zhang S, Liu Q, Hu X (2020b) Evolution of the functionalities and structures of biochar in pyrolysis of poplar in a wide temperature range. *Bioresour Technol* 304:123002. <https://doi.org/10.1016/j.biortech.2020.123002>
- Zhang X, Zhang P, Yuan X, Li Y, Han L (2020c) Effect of pyrolysis temperature and correlation analysis on the yield and physicochemical properties of crop residue biochar. *Bioresour Technol* 296:122318. <https://doi.org/10.1016/j.biortech.2019.122318>
- Zhang P, Wang X, Xue B, Huang P, Hao Y, Tang J, Maletić SP, Rončević SD, Sun H (2021a) Preparation of graphite-like biochars derived from straw and newspaper based on ball-milling and TEMPO-mediated oxidation and their supersorption performances to imidacloprid and sulfadiazine. *Chem Eng J* 411:128502. <https://doi.org/10.1016/j.cej.2021.128502>
- Zhang X, Zheng H, Wu J, Chen W, Chen Y, Gao X, Yang H, Chen H (2021b) Physicochemical and adsorption properties of biochar from biomass-based pyrolytic polygeneration: effects of biomass species and temperature. *Biochar*. 3:657–670. <https://doi.org/10.1007/s42773-021-00102-5>
- Zhang C, Yang R, Sun M, Zhang S, He M, Tsang DCW, Luo G (2022a) Wood waste biochar promoted anaerobic digestion of food waste: focusing on

- the characteristics of biochar and microbial community analysis. *Biochar*. 4:62. <https://doi.org/10.1007/s42773-022-00187-6>
- Zhang G, Feng Q, Hu J, Sun G, Evrendilek F, Liu H, Liu J (2022b) Performance and mechanism of bamboo residues pyrolysis: gas emissions, by-products, and reaction kinetics. *Sci Total Environ* 838:156560. <https://doi.org/10.1016/j.scitotenv.2022.156560>
- Zhang Y, Li M, Lu S (2022c) Rational design of covalent bond engineered encapsulation structure toward efficient, long-lived multicolored phosphorescent carbon dots. *Small* 19:2206080. <https://doi.org/10.1002/sml.202206080>
- Zhang S, Li B, Zhou J, Shi J, He Z, Zhao Y, Li Y, Shen Y, Zhang Y, Wu S (2023) Kill three birds with one stone: Mitochondria-localized tea saponin derived carbon dots with AIE properties for stable detection of HSA and extremely acidic pH. *Food Chem* 405:134865. <https://doi.org/10.1016/j.foodchem.2022.134865>
- Zhao Z, Wu Q, Nie T, Zhou W (2019) Quantitative evaluation of relationships between adsorption and partition of atrazine in biochar-amended soils with biochar characteristics. *Rsc Adv* 9:4162–4171. <https://doi.org/10.1039/c8ra08544g>
- Zhao T, Li S, Liu F, Wang Z, Wang H, Liu Y, Tang X, Bai M, Zhang M, Ma Y (2022) Molten-Li infusion of ultra-thin interfacial modification layer towards the highly-reversible, energy-dense metallic batteries. *Energy Storage Mater*. 45:796–804. <https://doi.org/10.1016/j.ensm.2021.12.032>
- Zherebker A, Rukhovich GD, Sarycheva A, Lechtenfeld OJ, Nikolaev EN (2022) Aromaticity index with improved estimation of carboxyl group contribution for biogeochemical studies. *Environ Sci Technol* 56:2729–2737. <https://doi.org/10.1021/acs.est.1c04575>
- Zhou X, Zhu Y, Niu Q, Zeng G, Lai C, Liu S, Huang D, Qin L, Liu X, Li B, Yi H, Fu Y, Li L, Zhang M, Zhou C, Liu J (2021) New notion of biochar: a review on the mechanism of biochar applications in advanced oxidation processes. *Chem Eng J* 416:129027. <https://doi.org/10.1016/j.cej.2021.129027>